X-ray and electron diffraction studies of superlattices and long-range three-dimensional Na ordering in γ-Na_xCoO_2 ($x=0.71$ and 0.84)

F.-T. Huang,[1,2,3] M.-W. Chu,[1,*] G. J. Shu,[1] H. S. Sheu,[4] C. H. Chen,[1] L.-K. Liu,[3] Patrick A. Lee,[5] and F. C. Chou[1,4]

[1]*Center for Condensed Matter Sciences, National Taiwan University, Taipei 106, Taiwan*

[2]*Taiwan International Graduate Program, Academia Sinica, Taipei 115, Taiwan*

[3]*Department of Chemistry, National Taiwan University, Taipei 106, Taiwan*

[4]*National Synchrotron Radiation Research Center, HsinChu 300, Taiwan*

[5]*Department of Physics, Massachusetts Institute of Technology, Cambridge, Massachusetts 02139, USA*

(Received 7 July 2008; published 12 January 2009)

We have recently demonstrated that $x=0.71$ and 0.84 are the two most stable single-phase compounds above $x=0.5$ in γ-Na_xCoO_2 [G. J. Shu *et al.*, Phys. Rev. B **76**, 184115 (2007); F. C. Chou *et al.*, Phys. Rev. Lett. **101**, 127404 (2008)], and this structural investigation was performed on the single crystals and pulverized samples elaborately synthesized therein. Using the complementary techniques of x-ray and electron diffractions, we unambiguously established the existence of superlattices in $x=0.71$ and 0.84, $\sqrt{12}a_p\times\sqrt{12}a_p\times 3c_p$, and $\sqrt{13}a_p\times\sqrt{13}a_p\times 3c_p$ (a_p and c_p, the hexagonal primitive cell parameters), respectively. The exceptionally large superlattice for $x=0.71$ arises from the long-range three-dimensional sodium ordering, consisting of the *spiral-like sodium-trimer chain* screwing along c axis and being decorated with alternating truncated-triangle and honeycomb sodium sublattices in *ab* plane. The trimers in the neighboring sodium planes show corner-shared-like characteristics along the chain direction. A larger interplane separation of the trimers that was expected to minimize the trimer interlayer Coulomb repulsion was, however, not observed, and all Co ions in the superlattice show similar charge characteristics. In $x=0.84$, the large superlattice is rather a result of the long-range ordering of *sodium monomers* both in *ab* plane and along c axis. The differences in the superlattice structure and the corresponding long-range sodium ordering between $x=0.71$ and 0.84 may provide the critical information in understanding their distinctly different physical properties from structural aspects.

DOI: 10.1103/PhysRevB.79.014413 PACS number(s): 75.50.−y, 61.05.cp, 61.05.jm, 61.50.Ah

I. INTRODUCTION

The hexagonal sodium cobaltate, γ-Na_xCoO_2 (space group $P6_3/mmc$), is characterized by a lamellar crystal structure that consists of edge-shared CoO_2 sheets sandwiching the sodium layer[1,2] with various x of $0.25\leq x\leq 0.84$.[3,4] The Na ions in the structure are distinguished by two crystallographic sites, Na1 and Na2. In contrast, there is only one crystallographic site for the Co ions, which form a triangular sublattice in *ab* plane with the trigonal-coordinated oxygen above and below the Co planes.[5–9] Na1 directly locates above and below the neighboring Co, whereas Na2 occupies the projected vacant center of the triangular Co sublattice.[5–9] Na2 has been suggested to be a more favorable site for the sodium,[5–8] and the partial occupancy of Na2 is indeed more significant than that of Na1 in the hexagonal unit cell with *disordered* Na1 and Na2 on the sodium plane.[5–9] The sum of the respective partial occupancies for Na1 and Na2 sites determines x.

In practice, the phase diagram of γ-Na_xCoO_2 can be separated into two parts, one for the Pauli-type paramagnetic metals with $0.25\leq x<0.5$ and the other for the Curie-Weiss metals with $0.5<x\leq 0.84$.[3,4] The most interesting material in the Pauli metal regime is $x\sim 1/3$ that exhibits an unexpected superconductivity upon further intercalation with water.[10] For $0.75\leq x\leq 0.84$ in the Curie-Weiss metal regime, the onset of a long-range A-type antiferromagnetic ordering (Co-intraplane ferromagnetic coupling and Co-interplane antiferromagnetic coupling) at ~22 K has been indicated,[11–13] and the enhanced thermoelectric power due to large spin entropy has been found and explained for ~0.84.[14] Intriguingly, the other Curie-Weiss metal, $x=0.71$, exhibits no magnetic ordering down to ~1.8 K.[3] The exactly half Na filled phase of $x=0.5$ is the only compound that shows a metal-to-insulator transition (MIT) near ~51 K.[3,4,15,16]

Indeed, the unique transport property for $x=0.5$ had stimulated a remarkable number of associated studies, leading to the discovery that the room-temperature crystal structure of $x=0.5$ shows an orthorhombic superlattice of $\sqrt{3}a_p\times 2a_p\times c_p$ (a_p and c_p, the hexagonal primitive cell parameters).[8,9,16,17] This orthorhombic supercell arises from the *two-dimensional* zigzag-chain ordering of Na1 and Na2 in the *ab* plane with the respective sodium sites fully occupied and is preserved down to 10 K without any further noticeable modifications.[8,9,16] In the superlattice of $x=0.5$, there are now two inequivalent crystallographic Co sites, Co1 (aligned with Na1 along c axis) and Co2, and these Co ions form Co1-Co2 stripelike patterns superimposed with the ordered Na1-Na2 zigzag chain when observing along c axis.[8,9,16] It is most interesting to notice that a unique antiferromagnetic ordering appears at MIT and is formed by the magnetically disordered-Co-ordered-Co stripe patterns,[17] consistent with the existence of Co1-Co2 stripes in the superlattice.[8,9,16] In addition, an electronically gapped ground state associated with MIT was suggested.[17] The *ab* plane two-dimensional sodium ordering in the orthorhombic superlattice of $x=0.5$ is, therefore, closely correlated with its various electronic instabilities.[3,4,17]

For $0.75\leq x\leq 0.84$ within the ionic context (charge localization[15]), it has been suggested that the existence of

A-type magnetic ordering near ~22 K is rather unexpectedly high considering the dilute spin-half Co^{4+} in the lattices.[12,13] The inelastic neutron scattering further indicated that the ferromagnetic intraplane and antiferromagnetic interplane exchange constants are nearly comparable, whereas a much smaller interplane magnitude was expected due to the lamellar structure of γ-Na_xCoO_2.[12,13] To account for these unexpected magnetic properties, the possible effect of sodium-ordering induced superlattices and itinerant charges deviating from the ionic context has been proposed[12,13] although the detailed superlattices remain to be elaborated. In $x=0.71$, the absence of the *A*-type magnetic ordering is also puzzling when taking into account that $x=0.71$ is compositionally close to the magnetically ordered $x=0.75$.[3,4,18,19] Moreover, $x=0.71$ is the only material in the Curie-Weiss-metal regime free from the *A*-type magnetic ordering,[3,4,18,19] and the existence of superlattice in $x\approx0.70$ (close to $x=0.71$ that we are considering) has also been suggested.[18,19] Indeed, it is generally believed that superlattices and their correlated sodium ordering should play an essential role in the various electronic ground states of the Curie-Weiss metal.[12,13,18–22] However, the associated detailed physical interplays remain to be an open question,[22] in sharp contrast to the better understood system for $x=0.5$.[3,4,17] Resolving the undetermined superlattices in the Curie-Weiss metals with and without the *A*-type magnetic ordering should shed more light on this question and is the goal of this paper.

In this work, we report the detailed structural characterization of $x=0.71$ and 0.84 using synchrotron x-ray and electron diffraction. All our structural investigations were performed at room temperature. Through our latest developments in the precise control of the sodium content in γ-Na_xCoO_2,[3] $x=0.71$ and 0.84 are the two most stable single-phase compounds above $x=0.5$ while the former shows no magnetic ordering down to ~1.8 K and the latter shows an *A*-type antiferromagnetic ordering near ~22 K.[4,18,19] We used these precisely controlled $x=0.71$ and 0.84 single crystals and pulverized powder samples for the structural studies. The sodium concentration has been verified by both the electron probe microanalysis, and the correlation between the *c* axis lattice constant and *x* to be consistently within error of 0.01.[3]

From single-crystal x-ray and electron diffraction studies, the existence of superlattices in $x=0.71$ and 0.84 was unambiguously indicated with the respective superperiodicity of $\sqrt{12}a_p\times\sqrt{12}a_p\times3c_p$ and $\sqrt{13}a_p\times\sqrt{13}a_p\times3c_p$. Further performing Rietveld analyses on the powder-diffraction patterns of $x=0.71$ and 0.84, the structural details of both superlattices were established, arising from the ordering of Na1 *trimers* [referred in Ref. 22 as Na2 trivacancy (**T**) and quadrivacancy (**Q**)] in $x=0.71$ and Na1 *monomers* (referred in Ref. 22 as Na2 divacancy) in $x=0.84$ both along *c* axis and in *ab* plane. The respective sodium ordering in $x=0.71$ and 0.84 is thus long range and three dimensional in nature, and the formation of Na1 trimers and monomers are mediated by the clustering of Na vacancies.[22,23] These sodium-ordering characteristics may provide structural hints to the intriguing magnetic interactions of γ-Na_xCoO_2 in Curie-Weiss metal regime with and without the *A*-type antiferromagnetic ordered ground state.[12,13,18,19]

II. EXPERIMENTAL

The synthesis of homogeneous and phase-pure γ-Na_xCoO_2 ($x=0.71$ and 0.84) single crystals with a precise control of the sodium content has been published elsewhere.[3] The powder samples for acquiring the synchrotron x-ray powder-diffraction data were pulverized from the single crystals and sealed in a 1-mm-diameter quartz capillary for the diffraction experiments. The pulverized sample of $x=0.84$ shows the single-phase characteristic. The powder of $x=0.71$, however, contains CoO and β-$Na_{0.6}CoO_2$ impurities, each around 4 wt %, which were not observed in the single crystals and may be introduced during the pulverization regardless of the cautions taken.

Single crystals with a dimension of $\sim2\times2\times0.1$ mm^3 were first examined in a transmission Laue geometry using the collimated synchrotron-radiation beam of 0.619 96 Å (diameter≈1 mm) with *c* axis parallel to the incident-beam direction. The synchrotron x-ray powder-diffraction patterns were acquired at the same beam line with the same wavelength and spot size. All synchrotron x-ray experiments were performed at the National Synchrotron Radiation Research Center, Taiwan. The structural characteristics of $x=0.71$ and 0.84 along *c* axis and in the whole reciprocal space were also investigated in house by the complementary technique of electron diffraction using a transmission electron microscope (TEM) (JEOL 2000FX), operated at 120 kV to reduce the beam-induced damages observed in γ-Na_xCoO_2 above 120 kV.[9] The electron diffraction investigations were performed on thin regions of the freshly cleaved single crystals, clamped in a Cu grid and immediately inserted into the TEM column. The general structure analysis system (GASA) program was exploited to analyze the powder-diffraction data using the Rietveld method with a pseudo-Voigt profile function.

III. RESULTS AND DISCUSSION

Figures 1(a) and 1(b) show the respective single-crystal transmission Laue diffraction results of $x=0.71$ and 0.84 along *c* axis, $[001]_p$ (*p*, the primitive hexagonal unit cell), indicating that sharp and periodic diffraction spots in addition to the intense Bragg reflections of the primitive unit cells, $(100)_p$ and $(010)_p$, are present throughout the patterns. Among approximately ten single crystals studied for each Na content, identical diffraction patterns with various qualities as shown in Figs. 1(a) and 1(b) were always observed. Further considering the spot size of the collimated beam as well as the characteristic lateral dimension and thickness of the single crystals, the diffraction patterns observed in Figs. 1(a) and 1(b) should reflect the intrinsic bulk characteristics of $x=0.71$ and 0.84, revealing the existence of superlattices in both phases.

Figures 1(a) and 1(b) indicated that the hexagonal-type repeated units [gray bold hexagons in the insets of Figs. 1(a) and 1(b)] characteristic to the primitive hexagonal symmetry of γ-Na_xCoO_2 are preserved, which corresponds to the real-space *ab* plane superperiodicity of $\sqrt{12}a_p\times\sqrt{12}a_p$ and $\sqrt{13}a_p\times\sqrt{13}a_p$ for $x=0.71$ and 0.84, respectively. The pres-

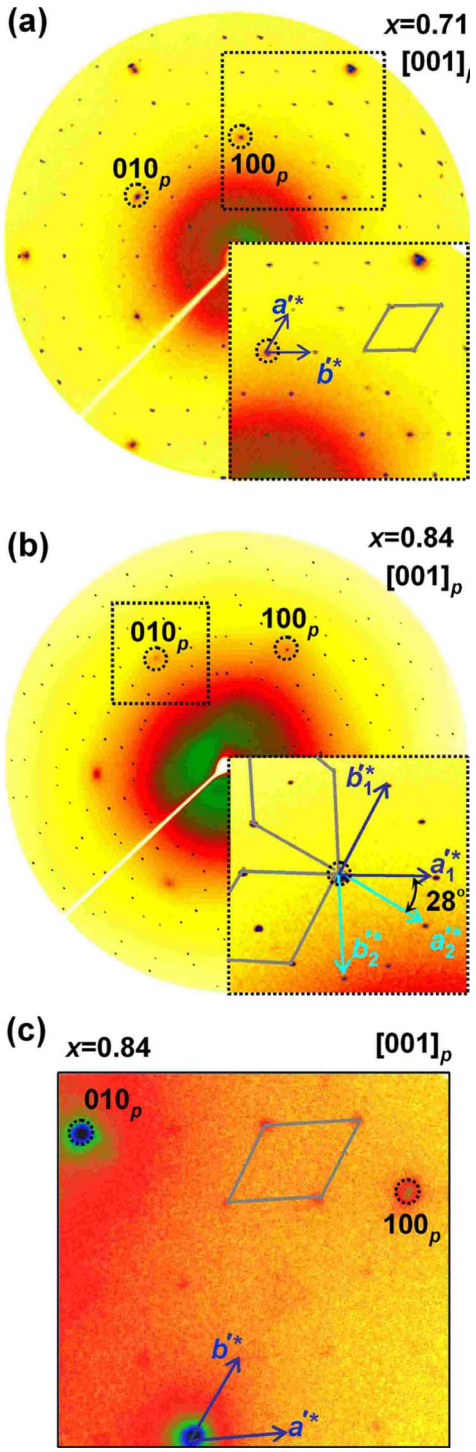

FIG. 1. (Color online) The transmission Laue x-ray diffraction patterns of (a) $x=0.71$ and (b) $x=0.84$ single crystals along c axis of the primitive cell $[001]_p$ (p, the primitive cell) reproduced from Ref. 22, showing the existence of superlattices ($a'^* \times b'^*$). The hexagonal-type repeated units of the superlattices are shown as solid gray hexagons in the insets of (a) and (b) and (c). Insets: the blow up of the respective dashed regions in (a) and (b). Inset of (b): the characteristic ringlike superlattice reflections of $x=0.84$, consisting of 12 diffraction spots due to the existence of two domains. (c) The single-domain diffraction feature of $x=0.84$ (domain size, at least ~150 nm) using SAED in an electron microscope.

ervation of the hexagonal-type repeated units suggests that upon the existence of these superlattices the corresponding symmetries of the respective phases could be lowered (e.g., orthorhombic in $x=0.5$) (Refs. 8, 9, and 16) but not down to any space groups other than the hexagonal or trigonal classes. In the inset of Fig. 1(b) for $x=0.84$, the ringlike features formed by 12 diffraction spots around the primitive Bragg reflections result from the coexistence of two mosaic superlattice domains, rotated by 28° to each other.[22] Using selected-area electron diffraction (SAED) with a beam-illumination area of ~150 nm in diameter for studying the different locations in the $x=0.84$ single crystal, the single-domain reflection feature of the superlattice, showing characteristically six out of the 12 reflections with a hexagonal-type repetition, were indeed regularly observed [Fig. 1(c)]. Figure 1(c) also suggests that the domain size is at least comparable to the illuminated area of ~150 nm. The two-domain superlattice characteristic of $x=0.84$ arises from the existence of two crystallographically equivalent choices for defining the superperiodicity of $\sqrt{13}a_p \times \sqrt{13}a_p$ over the primitive cell network. In contrast, there exists only one crystallographic choice for the superperiodicity in $x=0.71$, thus observed as the single-domain superlattice [Fig. 1(a)]. The detailed structural analyses of $x=0.71$ and 0.84 are shown in Secs. III A–III C.

A. Structural characterization of $x=0.71$

Figure 2 shows the representative SAED patterns of $x=0.71$ in three different orientations, $[001]_p$, $[201]_p$, and $[211]_p$. In Fig. 2(a), we can observe that there exists an ab plane modulation with the elementary vector of $1/6[110]_p$, which is equivalent to a superlattice modulation of $\sqrt{12}a_p \times \sqrt{12}a_p$ in real space as revealed in Fig. 1(a). In Figs. 2(b) and 2(c), the reciprocal-space projection directions provide further structural characteristics of $x=0.71$ in the third dimension (c axis). Such diffraction features are difficult to obtain from our Laue diffraction setup.

In Figs. 2(b) and 2(c), superlattice modulations in addition to the intense Bragg reflections of the primitive phase were also observed. All SAED patterns in Fig. 2 were uniformly observed over the large thin areas of the cleaved crystal, whereas the superlattice reflections of the given areas irreversibly vanished after being exposed to the electron beam over 5 min. In contrast, the intensity of the primitive Bragg reflections remains nearly unaffected. Such a facile radiation damage of the superlattice reflections suggests that the superlattice should arise from the ordering of the most mobile sodium ions in the lattice.[9] However, the complete indexing of all superlattice spots in Figs. 2(b) and 2(c) would require the tripling of c axis in addition to the ab plane superperiodicity characterized in Figs. 1(a) and 2(a), altogether leading to $\sqrt{12}a_p \times \sqrt{12}a_p \times 3c_p$. This exceptionally large three-dimensional superlattice has never been documented in $x=0.71$, and the corresponding volume (36 times of the primitive cell) is far more significant than what is usually observed for a superlattice such as a few times larger in $x=0.5$,[8,16] Fe_3O_4,[24] and $AgNiO_2$.[25]

Using $\sqrt{12}a_p \times \sqrt{12}a_p \times 3c_p$, the careful indexing of all diffraction spots in Fig. 2(b) further revealed the presence of

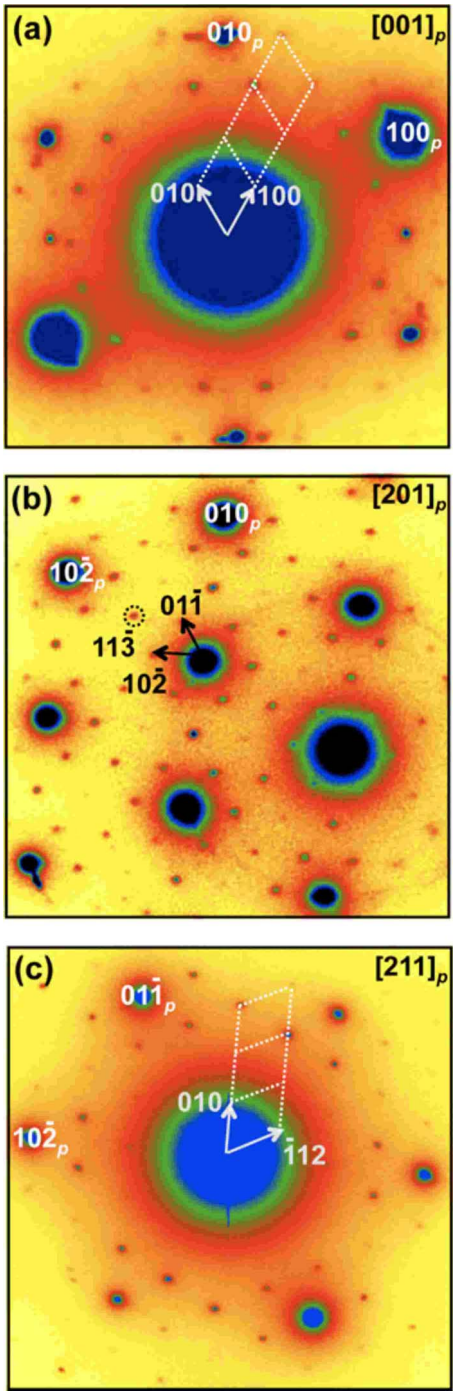

FIG. 2. (Color online) The SAED patterns of $x=0.71$ along the zone axes of (a) $[001]_p$, (b) $[201]_p$, and (c) $[211]_p$ (p, the primitive cell), altogether indicating the superlattice of $\sqrt{12}a_p\times\sqrt{12}a_p\times 3c_p$. The reflections without the p subscript are those indexed by the superperiodicity of $\sqrt{12}a_p\times\sqrt{12}a_p\times 3c_p$.

(113)-type reflections at odds to the extinction condition, hhl (l=even), of the primitive space group $P6_3/mmc$. The persistent existence of these symmetry forbidden reflections upon sample off-axis tilting suggests that they are not a consequence of the electron multiple scattering, giving a direct evidence for the breakdown of $6_3/m$ and c elements in $P6_3/mmc$ of primitive γ-Na_xCoO_2.[26] In the superlattice of

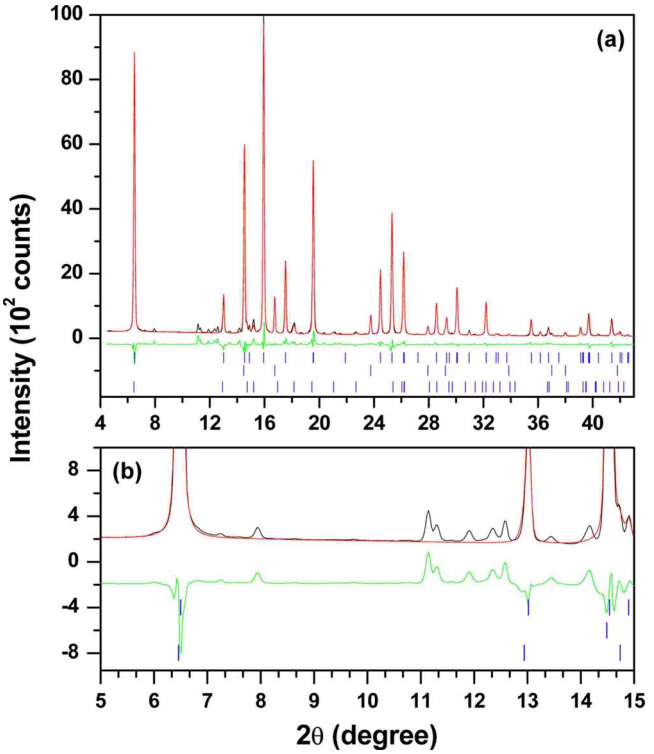

FIG. 3. (Color online) (a) The Rietveld refined plot of $x=0.71$ using the structural model of the primitive cell ($a_p\times a_p\times c_p$). The observed, calculated, and difference intensities are given as black, red, and green curves, respectively. The three sets of blue vertical bars indicate the Bragg conditions for $x=0.71$ (top), CoO (middle), and β-$Na_{0.6}CoO_2$ (bottom), respectively. (b) An enlarged region of (a), indicating the existence of superlattice reflections that cannot be described by the primitive cell.

$x=0.71$, a pronounced change in the coordination environments of Na1 and Na2 and/or the associated Co-O bonding characteristics upon the sodium ordering should be responsible for this symmetry reduction. We performed the Rietveld analyses of the powder-diffraction patterns to extract the related structural details.

Figure 3(a) shows the Rietveld refined plot of $x=0.71$ using first a structural model based on the primitive lattice ($P6_3/mmc$; Table I) with the disordered Na1 and Na2, the cell of $a_p\times a_p\times c_p$, and the Na2 site ($2d$) centered on the projected triangular Co sublattice. This disordered model (Table I), exploited in most Rietveld analysis reports of γ-Na_xCoO_2,[5–7,27] results in a significant amount of reflections remaining undetermined [not impurity contributions; Fig. 3(b)]. These features indicate that the structure of the primitive lattice is improper for describing the powder-diffraction pattern of $x=0.71$. Allowing off-center displacements of Na2($6h$) in the same space group $P6_3/mmc$, as found in certain γ-Na_xCoO_2,[5–7] cannot resolve the undetermined reflections due to the identical symmetry taken into account. Considering the observed hexagonal-type repeated units [Fig. 1(a)], the c-axis tripling [Figs. 2(b) and 2(c)], and the symmetry-element breakdown [Fig. 2(b)] in $x=0.71$, the space group of the superlattice should be then reduced from the primitive $P6_3/mmc$ to hexagonal $P6_2$ ($P6_4$ counterpart ignored for simplicity) or trigonal $P3_1$ ($P3_2$ counterpart also

TABLE I. The refinement results of $Na_{0.71}CoO_2$ and $Na_{0.84}CoO_2$ using the primitive cell model ($a_p \times a_p \times c_p$; $P6_3/mmc$) and the superlattice model ($P3_1$). In the primitive cell, the crystallographic sites of the constituent ions are Co($2a$), Na1($2b$), Na2($2d$), and O($4f$), and z of O is the only parameter that can be refined. The site occupancy in the structural models is denoted as n.

	$Na_{0.71}CoO_2$	$Na_{0.84}CoO_2$	$Na_{0.71}CoO_2$	$Na_{0.84}CoO_2$
Structural model	$a_p \times a_p \times c_p$	$a_p \times a_p \times c_p$	$\sqrt{12}a_p \times \sqrt{12}a_p \times 3c_p$	$\sqrt{13}a_p \times \sqrt{13}a_p \times 3c_p$
a (Å)	2.8287(1)	2.8448(1)	9.7991(1)	10.2569(1)[a]
c (Å)	10.9373(5)	10.9539(5)	32.8111(1)	32.853(1)
V (Å^3)	75.795(4)	76.775(5)	2728.6(1)	2993.2(1)
CoU_{iso} (Å$^2 \times 10^2$)	1.6(1)	2.1(1)	1.5(1)	
Na1U_{iso} (Å$^2 \times 10^2$)	5.9(10)	10.0(12)	2.5[b]	
n	0.21(3)	0.24(4)	1[b]	
Na2U_{iso} (Å$^2 \times 10^2$)	5.9(10)	10.0(12)	2.5	
n	0.50(2)	0.58(3)	1	
Oz	0.0922(5)	0.0932(5)	[c]	
OU_{iso} (Å$^2 \times 10^2$)	2.2(3)	2.1(2)	1.9(1)	
R_p (%)	6.95	5.14	6.30	3.02
R_{wp} (%)	10.53	8.21	8.91	5.18
χ^2	3.549	4.896	2.561	1.947
Average bond length (Å)				
⟨Co-O⟩	1.923(3)	1.933(6)	1.920(3)[c]	
⟨Na1-O⟩	2.372(2)	2.377(4)	2.375(2)	
⟨Na2-O⟩	2.372(2)	2.377(4)	2.375(2)	

[a]Due to the quality issue of the diffraction pattern after pulverizations (see text), the detailed Rietveld refinements of the various superlattice structural models were not conclusive and only the profile fitting can be reliably performed.

[b]In the superlattice of $x=0.71$, there are 17 crystallographic sites for the Na ions, either aligned with Co-type Na1 in the primitive cell or locating in the center of the triangular Co sublattices such as Na2. In the superlattices, we thus keep the expressions of Na1 and Na2 for simplicity and each sodium site is entirely full. ADPs of Na1 and Na2 were fixed.

[c]In the superlattice of $x=0.71$, the respective atomic positions were derived from those in the primitive cell. Na and O show negligible displacements from the parent positions in the primitive cell upon refinements. The number of O in the superlattice is too large, and we use the average bond lengths of all CoO_6 octahedra and NaO_6 prisms to represent the refined results of the atomic positions.

ignored).[26] The remarkable volume of the superlattice in $x=0.71$ suggests that the associated sodium ordering should be described by a large number of crystallographically independent atoms. Compared to $P6_2$, the lower-symmetry $P3_1$ with the least correlations among the given atoms (i.e., more crystallographic atoms needed to describe the superlattice) was, therefore, chosen. Otherwise, a superlattice with a smaller volume and a higher averaged symmetry, thus less crystallographically independent atoms, could have been proposed such as the case in the superlattice of Fe_3O_4.[24]

B. Long-range three-dimensional sodium ordering in $x=0.71$

The construction of the three-dimensional sodium-ordering model in $x=0.71$ for further Rietveld analyses should be consistent with the symmetry $P3_1$ indicated in Sec. III A. Considering the lamellar structure of γ-Na_xCoO_2, the construction can be simplified as a stacking of the alternating sodium ordered layers interpenetrating with the CoO_2 sheets as its two-dimensional counterpart, $\sqrt{12}a_p \times \sqrt{12}a_p \times c_p$, elucidated here below.

In the primitive lattice of γ-Na_xCoO_2 [Fig. 4(a)], two sodium layers are present in the structure. Due to the feature coordination of oxygen to Co, the Na2-oxygen prism characteristic to the top sodium layer locates on the left triangular Co sublattice, whereas that to the bottom sodium layer locates on the right [Fig. 4(a)] with an inversion feature related to each other.[5–7,27] This characteristic is easily revealed when projecting the respective sodium layers on the Co sublattices along c axis [Fig. 4(b)]. In addition, the crystallographic interatomic distance between the nearest neighbored Na1 and Na2 is ~1.64 Å, smaller than the ionic size of the sodium ion itself (radius of ~1.02 Å).[23,28] This spatial feature suggests that, upon sodium ordering, the occupancy of a given Na1 (Na2) position would exclude three nearby Na2 (Na1). The nominal stoichiometry, $x=0.71$, must be also maintained in the sodium-ordering model. All these features have impor-

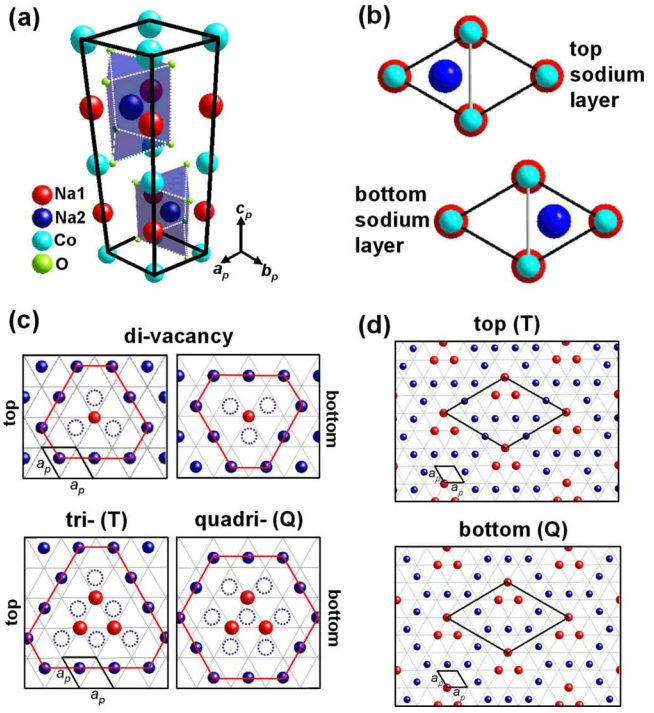

FIG. 4. (Color online) (a) The unit cell of a primitive lattice, and (b) the top and bottom sodium layers of the lattice projected along c axis. (c) The schemes for the Na1 monomer and the Na1 trimer. The Na1 monomer is assisted by the divacancy clustering, and the Na1 trimer is mediated by the respective **T** and **Q** clusterings on the top and bottom sodium layers. The dashed blue circles indicate the Na2 vacancies. Note the truncated-triangle (honeycomb) Na2 sublattice on the top (bottom) sodium layer in the Na1 trimer (see the solid red). The Na2 sublattices in the Na1 monomer are both truncated-triangle type (see the solid reds). (d) The scheme for a superlattice of $\sqrt{12}a_p \times \sqrt{12}a_p \times c_p$ assisted by the ordering of Na1 trimers in the respective top (**T**) and bottom (**Q**) sodium layers. In (c) and (d), Co and O are ignored for simplicity.

tant consequences on the following superlattice constructions.

The phase of $x=0.71$ can be considered as the doping of sodium vacancies (0.29) to $NaCoO_2$, where presumably all sodium ions occupy only the Na2 site, thus Na2-vacancy being introduced.[23] At the first approximations, the individual Na2 vacancies must be diluted periodically in the Na2 matrix so as to account for the superperiodicity ($\sqrt{12}a_p \times \sqrt{12}a_p \times c_p$ for now). Nevertheless, the multivacancy clustering [Fig. 4(c)], which involves Na1, had been demonstrated to be a more energetically favorable manner in mediating the superlattices than the periodic arrangements of individual Na2 vacancies alone.[23] Figure 4(c) depicts the associated divacancy, trivacancy, and quadrivacancy clusters, which are assisted by the delicate balance of the Coulomb interactions among Na1, Na2, and Na2 vacancies through promoting Na2 nearby the Na2 vacancies to Na1 as proposed by Roger *et al.*[23] The divacancy cluster [top panel of Fig. 4(c)], therefore, consists of three Na2 vacancies surrounding a Na1 monomer ($3-1=2$, thus divacancy). The trivacancy and quadrivacancy clusters [bottom panel of Fig. 4(c)] are then the result of the Na1 trimer being surrounded by six ($6-3=3$, thus trivacancy) and seven Na2 vacancies ($7-3=4$, thus quadrivacancy), respectively. Note that the Na1-Na1 spacing in the Na1 trimer is of ~2.83 Å ($\approx a_p$). The existence of divacancy clusters at the top and bottom sodium layers leads to Na1 monomers decorated with the respective truncated-triangle Na2 sublattices that are inversely symmetric to each other [solid red in the top panel of Fig. 4(c)]. This inversion symmetry is characteristic to the Na2-oxygen prisms in γ-Na_xCoO_2 [Figs. 4(a) and 4(b)]. Such an inversion operation between the top and bottom Na2-oxygen prisms, however, naturally results in distinct vacancy numbers at the top (**T**) and bottom (**Q**) sodium layers for the given Na1 trimer [bottom panel of Fig. 4(c)], which was not particularly documented when it first appeared in Ref. 23. The vacancy imbalance at the **T** and **Q** sodium layers, although both visualized as a Na1 trimer [bottom panel of Fig. 4(c)], is indeed a natural consequence dictated by the inverse symmetry of the Na2-oxygen prisms in γ-Na_xCoO_2. Therefore, **T** and **Q** layers always appear simultaneously, and the arbitrary in-plane shifts of the trimers do not affect the **T** and **Q** characters of the corresponding sodium layers. It should be also noted that the Na1 trimers at **T** and **Q** layers are decorated with Na2 sublattices of different geometries, truncated-triangle and honeycomb, respectively, as seen in the bottom panel of Fig. 4(c) (solid red).

In the superlattice of $\sqrt{12}a_p \times \sqrt{12}a_p \times c_p$, the long-range sodium ordering by the periodic arrangements of Na1 monomers in any plausible patterns would lead to identical x of 10/12 ~0.833.[29] The thus-derived x is inconsistent with the nominal stoichiometry of $x=0.71$, and the appearance of the superlattice due to Na1 monomer ordering is accordingly ruled out. In contrast, the sodium ordering by Na1 trimers features the combination of **T** and **Q** sodium layers in the superlattice [schematic of Fig. 4(d); trimers showing an interlayer in-phase stacking; see also the text later], giving rise to $x \approx 1/2(9/12+8/12) \approx 0.708$ in remarkable consistence with $x=0.71$. The Na1 trimers and the decorating truncated-triangle and honeycomb Na2 sublattices all exhibit a threefold symmetry along c axis, also consistent with the threefold characteristic of $P3_1$ derived in Sec. III A. This Na1-trimer ordering model for the superlattice of $\sqrt{12}a_p \times \sqrt{12}a_p \times c_p$ is satisfactory so far.

The experimentally observed tripling of c axis [Figs. 2(b) and 2(c)] indicates that the Na1 trimers also order along this direction. A simple interlayer in-phase stacking of the Na1 trimers along c axis [schematic of Fig. 5(a)], however, provides no obvious driving force for the c-axis tripling. An arbitrary interlayer out-of-phase stacking of the trimers in **T** and **Q** layers would otherwise expect a less significant modulation along c axis (e.g., c-axis doubling) because the superlattice with a smaller supercell volume is always more energetically favorable.[24] Note also that the derived $x \approx 0.708-0.71$ is persistent to the c-axis tripling and the interlayer out-of-phase shifting of the trimers. The threefold symmetry along c axis proposed by the electron diffraction ($P3_1$, III A) thus suggests that the Na1-trimer ordering in the observed superlattice, $\sqrt{12}a_p \times \sqrt{12}a_p \times 3c_p$, should exhibit a well-defined interlayer correlation.

Due to the tripled c axis in $\sqrt{12}a_p \times \sqrt{12}a_p \times 3c_p$, there are now three **T** and three **Q** sodium layers in the superlattice

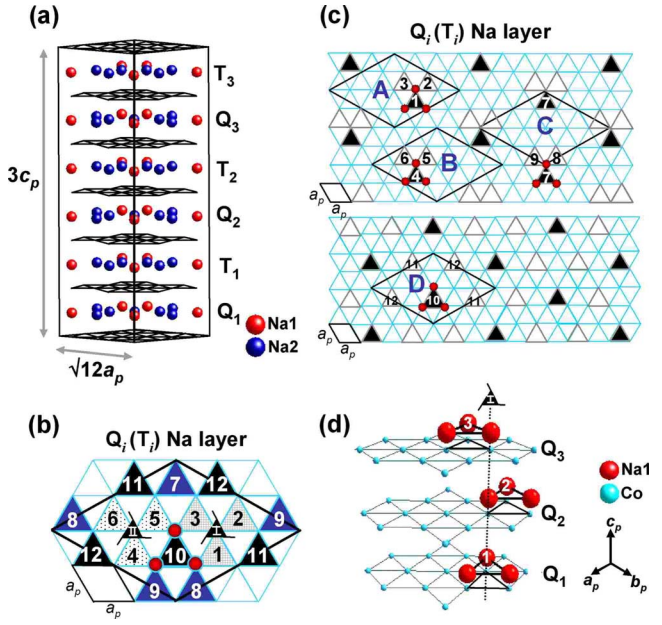

FIG. 5. (Color online) (a) A simple structural model for the $\sqrt{12}a_p \times \sqrt{12}a_p \times 3c_p$ superlattice of $x=0.71$, consisting of the stacking of six sodium layers, $\mathbf{Q}_i$ and $\mathbf{T}_i$, ($i=1$, 2 and 3) with the trimers aligned in phase along c axis. Co and O are ignored for simplicity. (b) The 12 available locations in an individual sodium layer of the superlattice, $\mathbf{Q}_i$ or $\mathbf{T}_i$, to accommodate the single Na1 trimer per layer. Due to the space group $P3_1$ of the superlattice, the threefold screw operation 3_1, centered on I and II, simplifies the 12 locations into four groups, A–D as shown in (c). The black triangle in (c) indicates the single trimer in each $\mathbf{Q}_i$ or $\mathbf{T}_i$ sodium layer of the superlattice, and those with gray edges reveal the trimers in each $\mathbf{Q}_{i+1,i+2}$ or $\mathbf{T}_{i+1,i+2}$ sodium layers. Here, $i=1$. Take group A, for example, the essence of the grouping in (b) and (c) is that allocating the Na1 trimer in $\mathbf{Q}_1$ ($\mathbf{T}_1$) layer at location 1 would indicate the presence of the Na1 trimer in $\mathbf{Q}_2$ ($\mathbf{T}_2$) layer at location 2 and the Na1 trimer in $\mathbf{Q}_3$ ($\mathbf{T}_3$) layer at location 3, also shown in (d). Na2 and O have been ignored in (d) for simplicity.

with one Na1 trimer per layer as shown in Fig. 5(a). For convenience, the respective sodium layers are termed as $\mathbf{Q}_i$ and $\mathbf{T}_i$ ($i=1$, 2, and 3) with the i order starting from the bottom of the superlattice [Fig. 5(a)]. In each individual $\mathbf{T}_i$ and $\mathbf{Q}_i$ layers, there are 12 possible locations for accommodating the single Na1 trimer, numbered in Figs. 5(b) and 5(c), as a result of the 12 primitive unit cells involved in the ab plane of the superlattice. This feature is not mentioned when first appearing in Fig. 4(d) for simplicity. At each indicated location, the Na1 trimer directly sits on top of the triangular Co sublattice of the primitive cell [e.g., the Na1 trimer at location 10 in Fig. 5(b); those at locations 1, 4, 7, and 10 in Fig. 5(c)].

In the superlattice, the threefold screw operation 3_1 of the feature symmetry $P3_1$ is centered on I and II [Fig. 5(b)] and characterized by a threefold rotation along c axis accompanied with an $c/3$ translation ($c=3c_p$).[26] This symmetry operation simplifies the above 12 locations and their complicated interlayer relationships into four groups: A–D, as visualized by numbers grouped with four different notations in Fig. 5(b) [see also Fig. 5(c)]. Allocating the single Na1 trimer in $\mathbf{Q}_1$ ($\mathbf{T}_1$) layer at location 1, the trimer in $\mathbf{Q}_2$ ($\mathbf{T}_2$) layer would appear at location 2 due to the 3_1 symmetry operation and the trimer in $\mathbf{Q}_3$ ($\mathbf{T}_3$) layer should be then present at location 3 also by symmetry, altogether leading to group A as shown in Figs. 5(c) and 5(d) (ignoring the presence of a $\mathbf{T}$ layer between two neighboring $\mathbf{Q}$ layers for simplicity). The same principle is obeyed in B-type $4(\mathbf{Q}_1)$-$5(\mathbf{Q}_2)$-$6(\mathbf{Q}_3)$, C-type $7(\mathbf{Q}_1)$-$8(\mathbf{Q}_2)$-$9(\mathbf{Q}_3)$, and D-type $10(\mathbf{Q}_1)$-$11(\mathbf{Q}_2)$-$12(\mathbf{Q}_3)$, shown in Fig. 5(c). The essence of this symmetry-derived grouping is then that knowing the location of the single Na1 trimer in $\mathbf{Q}_i$ ($\mathbf{T}_i$) layer would guide one to the rest in the other $\mathbf{Q}$ ($\mathbf{T}$) layers that are decorated with the honeycomb (truncated-triangle) Na2 sublattices. On the basis of the first choice for the trimer location in respective $\mathbf{Q}_1$ and $\mathbf{T}_1$ layers, there are, therefore, 13 different combinations for the $\mathbf{Q}_{1,2,3}$ and $\mathbf{T}_{1,2,3}$ sodium layers to account for the c-axis tripling, such as A($\mathbf{Q}$)-B($\mathbf{T}$) of $1(\mathbf{Q}_1)$-$4(\mathbf{T}_1)$-$2(\mathbf{Q}_2)$-$5(\mathbf{T}_2)$-$3(\mathbf{Q}_3)$-$6(\mathbf{T}_3)$ and A($\mathbf{Q}$)-C($\mathbf{T}$) of $1(\mathbf{Q}_1)$-$7(\mathbf{T}_1)$-$2(\mathbf{Q}_2)$-$8(\mathbf{T}_2)$-$3(\mathbf{Q}_3)$-$9(\mathbf{T}_3)$.[29] In two neighboring $\mathbf{Q}_i$-$\mathbf{Q}_{i+1}$ or $\mathbf{T}_i$-$\mathbf{T}_{i+1}$ sodium layers, the in-plane interlayer separation between the individual trimers is $\approx a_p$ for groups A–C and $\approx 2a_p$ for group D [Figs. 5(b)–5(d)]. In two closely neighboring $\mathbf{T}_i$ and $\mathbf{Q}_i$ layers, the in-plane interlayer separation between the individual Na1 trimers can thus be $\approx a_p$, $\approx \sqrt{3}a_p$, or $\approx 2a_p$, depending on the combination of the sodium layers among the 13 possible choices.

We then performed the Rietveld analyses of the above 13 structural models that take into account the three-dimensional sodium ordering ($P3_1$; 89 crystallographic atoms; 17, Na; 24, Co; 48, O), and these models were constructed on the basis of the atomic parameters in the primitive lattice derived from Fig. 3 ($a_p \times a_p \times c_p$; see also Table I). All the previously undetermined reflections in Fig. 3 can now be described by the extinction conditions of $P3_1$ in the superlattice, $\sqrt{12}a_p \times \sqrt{12}a_p \times 3c_p$ (Fig. 6). In each exceptionally large superlattice model, the refinements of all atomic positions and atomic displacement parameters (ADPs) (U_{iso}) of the 89 atoms typical for Rietveld refinements can, however, lead to divergences due to the strong numerical correlations in large- and low-symmetry cells such as in the current cases.[24] Although there are 17 crystallographic Na sites in the superlattice of $x=0.71$, these sites are either aligned with Co (six of them) such as Na1 in the primitive cell or locate in the center of the triangular Co sublattices (eleven of them) such as Na2. We thus keep the expressions of Na1 and Na2 hereinafter for simplicity. For the refinement of each superlattice model, ADPs of all Co and O ions were first constrained, respectively, and allowed to be refined. ADPs of all Na ions were, however, fixed at a reasonable value (Table I). After the ADP refinements of Co and O, the atomic positions of Na2 and O nearby the Na1 trimers were then independently refined, followed by the independent refinements of those of all the other Na2 and O, and Na1. The atomic positions of Co are not to be refined as in the primitive lattice.[5–7,27] This refinement method effectively reduces the numerical correlations and gives a consistent description of the reflection intensities revealed in the experimental diffraction pattern (Fig. 6).

Among the 13 structural models, only the refined A($\mathbf{Q}$)-D($\mathbf{T}$) combination of $1(\mathbf{Q}_1)$-$11(\mathbf{T}_1)$-$2(\mathbf{Q}_2)$-$12(\mathbf{T}_2)$-

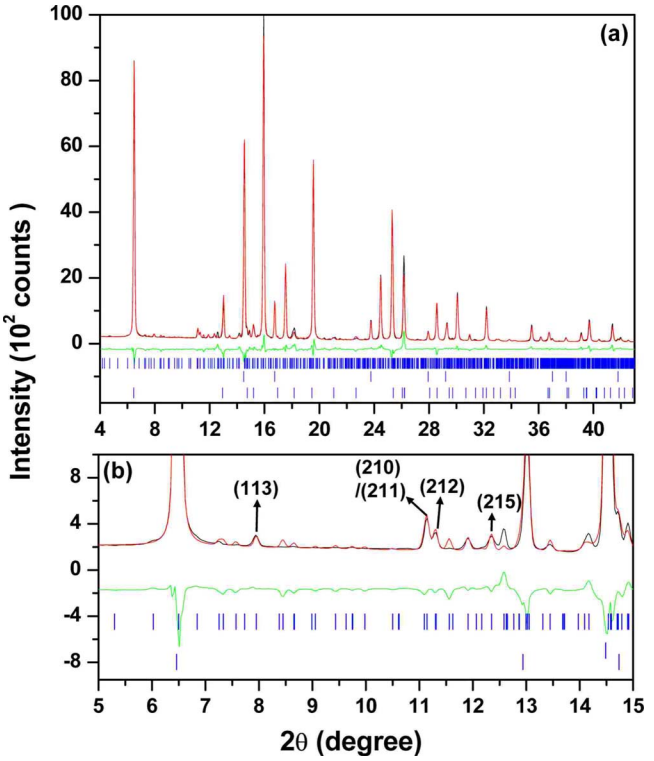

FIG. 6. (Color online) (a) The Rietveld refined plot corresponding to the refined superlattice structure of $x=0.71$ in Fig. 7. The observed, calculated, and difference intensities are given as black, red, and green curves, respectively. The three sets of blue vertical bars indicate the Bragg conditions for $x=0.71$ (top), CoO (middle), and β-$Na_{0.6}CoO_2$ (bottom), respectively. (b) An enlarged region of (a), showing that both the positions and the intensities of the superlattice peaks can be described by the superlattice structure in Fig. 7.

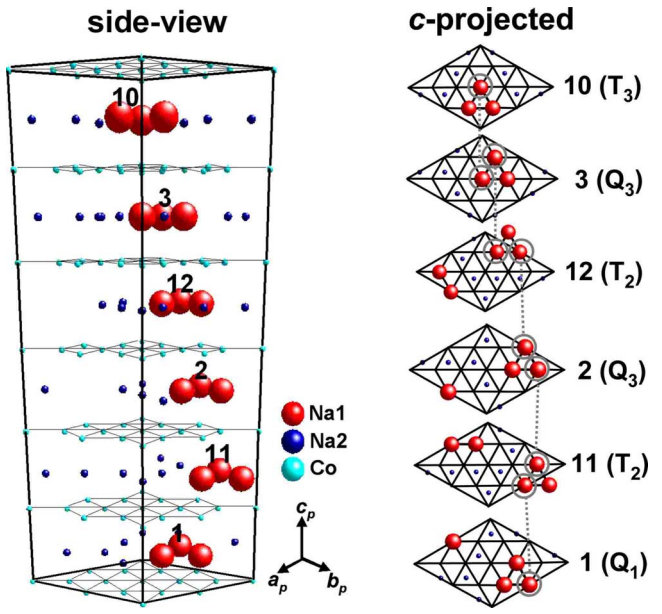

FIG. 7. (Color online) The refined long-range three-dimensional sodium ordering in $x=0.71$ ($\sqrt{12}a_p \times \sqrt{12}a_p \times 3c_p$), characterized by the Na1-trimer chain that screws along c axis. The Na1-trimer chain shows the trimer periodicity of $1(\mathbf{Q}_1)$-$11(\mathbf{T}_1)$-$2(\mathbf{Q}_2)$-$12(\mathbf{T}_2)$-$3(\mathbf{Q}_3)$-$10(\mathbf{T}_3)$, side view (left panel) and c projected (right panel). The gray circles and dashed lines in the right panel are guides for the eyes to reveal the interlayer corner-shared-like characteristics of the Na1 trimers and also the screwing operation of the trimers. O (side view and c projected) and/or Co (c projected) are ignored for simplicity. The size of Na1 has been exaggerated for improving the figure readability.

$3(\mathbf{Q}_3)$-$10(\mathbf{T}_3)$ (Fig. 7) can achieve both the fair goodness of fit (Table I) and the satisfactory intensity descriptions of all superlattice reflections [e.g., (113), ~7.95°; Figs. 6(a) and 6(b)], which are one to two orders weaker than the strong reflections ascribed to the CoO_2 sheets [e.g., (006), 6.499°; (220), 14.54°; (226), 15.94°; Fig. 6(a)]. In the refinement, the atomic positions of Na1, Na2, and O show negligible displacements from the values derived from the primitive lattice (Table I). More importantly, the calculated intensities of all superlattice reflections [e.g., (210), ~11.09°; (211), ~11.14°; (212), ~11.30°; (215), ~12.35°; Fig. 6(b)] vanish upon the removal of the Na1 trimers in the A(**Q**)-D(**T**) combination (without modifying the Na2 sublattices), firmly establishing the essential role played by the Na1 trimers in the superlattice. In $x=0.71$, the existence of the exceptionally large superlattice due to a long-range three-dimensional sodium ordering should be confirmative. The most promising feature of this refined sodium ordering is its spiral-like Na1-trimer chain that screws along c axis (left panel of Fig. 7), and is decorated with alternating honeycomb ($\mathbf{Q}_i$) and truncated-triangle ($\mathbf{T}_i$) Na2 sublattices in ab plane (right panel of Fig. 7), in certain resemblance to a single-strand deoxyribonucleic acid (DNA) decorated with different bases along the axial direction.[30]

In closely neighboring $\mathbf{T}_i$ and $\mathbf{Q}_i$ layers of the ordered Na1 chain, the trimers surprisingly exhibit an in-plane interlayer separation of $\approx a_p$, and always share a corner with those in the nearest neighboring sodium planes (see the guiding gray circles and dashed lines; right panel of Fig. 7). The larger interlayer trimer separation of $\approx\sqrt{3}a_p$ for the other A(**Q**)-D(**T**) combination, $1(\mathbf{Q}_1)$-$12(\mathbf{T}_1)$-$2(\mathbf{Q}_2)$-$10(\mathbf{T}_2)$-$3(\mathbf{Q}_3)$-$11(\mathbf{T}_3)$ and that of $\approx 2a_p$ for a D(**Q**)-D(**T**) combination of $12(\mathbf{Q}_1)$-$11(\mathbf{T}_1)$-$10(\mathbf{Q}_2)$-$12(\mathbf{T}_2)$-$11(\mathbf{Q}_3)$-$10(\mathbf{T}_3)$, propitious for their minimization of the interplane Coulomb repulsion,[23] however, give unsatisfactory refinements due to their poor descriptions of the intensity of the superlattice reflections. The above experimental observations lead to two important remarks. First, the possible Coulomb screening effect of the CoO_2 sheets could be excluded. If it were indeed predominant, the interlayer Na1-trimer chain ordering (Fig. 7) should have been frustrated. Second, the origin for the Na1-trimer chain ordering with a trimer interlayer separation of $\approx a_p$ should be beyond a simple Coulomb repulsion consideration[23] that expects a larger separation such as $\approx\sqrt{3}a_p$ or $\approx 2a_p$ otherwise.

Further examination of CoO_6 right above or below the Na1 trimers and the other octahedra in the refined superlattice as shown in Fig. 7 indicated that the average Co-O bond lengths of all these octahedra, within the estimated standard deviations, can be considered to be identical (Table I), as

reflected in the mentioned negligible displacements of O from the positions derived from the primitive lattice. The associated bond-valence-sum (BVS) estimations then revealed that the valences of the Co ions in the superlattice are all similar, ~3.31 (in remarkable agreement with the nominal valence of ~3.29), without noticeable charge separations such as Co^{3+} or Co^{4+}. A lower (higher) charge for metal ions is reflected on the corresponding longer (shorter) metal-oxygen bonds.[24,25] The Co ions right above or below Na1 in this material were reported to possess a much lower valence than the others, i.e., charge ordered,[18,19] and the associated CoO_6 octahedra should accordingly be larger than that of the others.[8,24] In the refined superlattice of $x=0.71$, all CoO_6 octahedra are nearly the same in size as characterized by their comparable average Co-O bond lengths and BVS values elucidated above. Our structural results do not suggest the existence of a charge ordering ground state at room temperature, and the Co ions sandwiched by Na1 of the corner-shared-like trimers in the superlattice (right panel of Fig. 7) do not show any visible charge differences compared to the others. The formation of the three-dimensional sodium ordering in $x=0.71$, therefore, seems not to be a result of mimicking the ionic potential of the Co triangular sublattices either.

Although we have elaborated the structural details of the superlattice in $x=0.71$, the profound driving force for its three-dimensional sodium ordering is still unclear and may have an electronic origin that remains to be explored. In $x=0.71$, the spiral-like Na1-trimer chain along c axis and the two kinds of alternating Na2 sublattices decorating the chain may provide structural hints to its absence of a magnetic ordering down to ~1.8 K,[3] also to be correlated with the possible electronic origin for the three-dimensional sodium ordering.

We were aware that the ordering of Na1 trimers similar to Fig. 7 had been reported in Ref. 23 (without the c-axis tripling) for describing a diffraction pattern such as Fig. 1(b) instead of Fig. 1(a) as we established. As demonstrated in Sec. III C, the superlattice and the suggested Na1-trimer ordering in Ref. 23 could be questionable.

C. Structural characterization and long-range three-dimensional sodium ordering in $x=0.84$

In the transmission Laue and electron diffraction investigations of $x=0.84$ [Figs. 1(b) and 1(c)], the ab plane superperiodicity of $\sqrt{13}a_p\times\sqrt{13}a_p$ has been established. The Rietveld refinement of the powder-diffraction pattern of $x=0.84$, using the primitive lattice, further indicated that there exists a significant number of weak superlattice reflections [Figs. 8(a) and 8(b); Table I], which cannot be taken into account without considering the c-axis tripling in addition to $\sqrt{13}a_p\times\sqrt{13}a_p$, thus $\sqrt{13}a_p\times\sqrt{13}a_p\times 3c_p$ [Fig. 8(c)]. Figure 8(c) shows the profile fitting result using both the superlattice of $\sqrt{13}a_p\times\sqrt{13}a_p\times 3c_p$ (Table I) and the most compatible space group of $P3_1$ as in $x=0.71$.

Compared to the Na1-trimer dominant phase of $x=0.71$, the exceptionally large superlattice of $x=0.84$, doped with less Na2 vacancies, should be dictated by the long-range three-dimensional ordering of the individual Na1 monomers

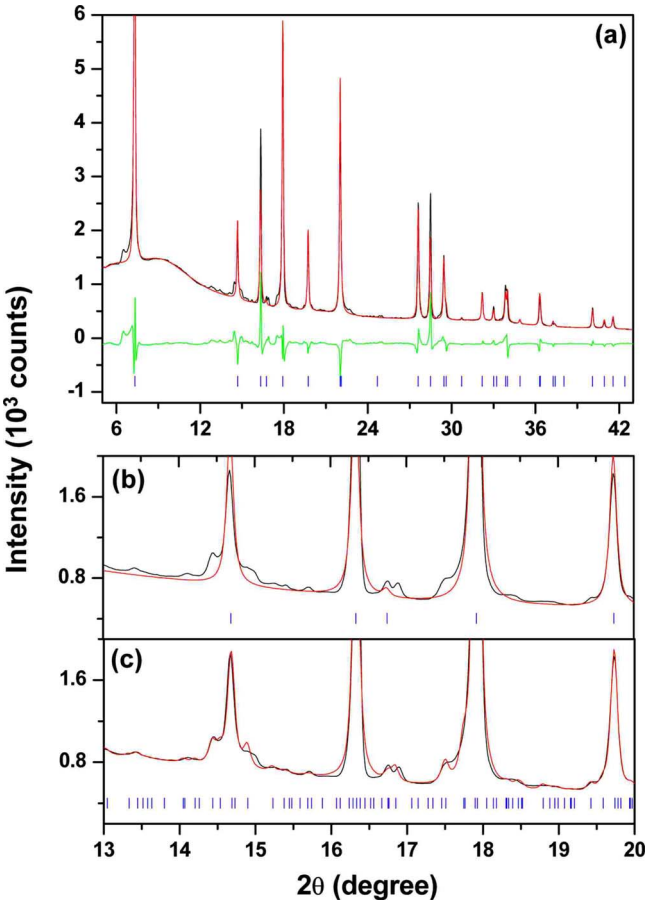

FIG. 8. (Color online) (a) The Rietveld refined plot of $x=0.84$ using the structural model of the primitive cell ($a_p\times a_p\times c_p$). The observed, calculated, and difference intensities are given as black, red, and green curves, respectively. The blue vertical bars indicate the Bragg conditions for $x=0.84$. (b) An enlarged region of (a), indicating the existence of superlattice reflections that cannot be described by the primitive cell. (c) The profile fitting result of $x=0.84$ using the superperiodicity of $\sqrt{13}a_p\times\sqrt{13}a_p\times 3c_p$ in $P3_1$, indicating that the undetermined reflections in (b) can now be described.

[divacancy clusters; top panel of Fig. 4(c)] in each of the six sodium layers of the superlattice. As indicated in Fig. 4(c) (top panel), the Na1 monomers give rise to identical vacancy numbers on the alternating sodium layers, in which the decorating Na2 sublattices are all truncated triangle like and inversely symmetric to each other. The existence of the Na1 monomers in the superlattice then leads to $x\approx 11/13\approx 0.846$, in good agreements with the nominal x of 0.84.

In the superlattice of $x=0.84$ ($\sqrt{13}a_p\times\sqrt{13}a_p\times 3c_p$), the Na1 monomers in the six sodium layers should also exhibit certain interlayer symmetric relationships, such as $x=0.71$, so as to result in the c-axis tripling. However, the superlattice peaks in the diffraction pattern of $x=0.84$ are very weak (<3% of the strong reflections of the primitive lattice), significantly convoluted to each other, and degraded by the broad maximum at 5°–15°, all shown in Figs. 8(a) and 8(c). These diffraction features are obviously dissimilar to the nicely independent and/or relatively stronger superlattice reflections in $x=0.71$ with a flat background, suitable for the

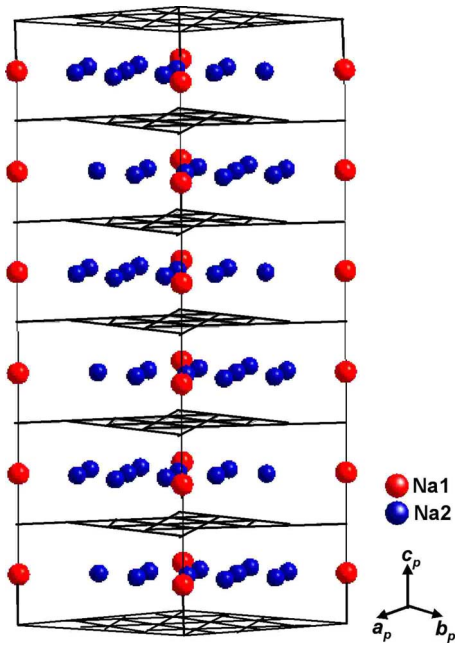

FIG. 9. (Color online) The proposed superlattice structure of $x=0.84$ ($\sqrt{13}a_p \times \sqrt{13}a_p \times 3c_p$) used to calculate Fig. 8(c), showing the single monomers in the respective six sodium layers aligned in-phase along c axis. Although the in-phase stacking of the monomers provides no obvious driving force for the c-axis tripling, the quality of the x-ray diffraction pattern [Fig. 8(a)] does not allow one to more specifically derive the exact ordering of the monomers in ab plane and along c axis such as the case in $x=0.71$ (see text).

detailed Rietveld refinements of the superlattice (Figs. 6 and 7). The detailed Rietveld determination of the long-range three-dimensional sodium ordering for $x=0.84$ is thus impractical although various structural models on the basis of the ordered Na1 monomers can still be proposed using the 3_1 symmetry operation of $P3_1$. The powder-diffraction experiments have been repeated for five times using five different pulverized samples while no obvious improvements compared to Fig. 8(a) can be achieved and the broad maximum was always present, most probably, ascribed to the unidentified amorphous background. In contrast, sharp superlattice reflections were always observed in the single-crystal x-ray diffraction studies of those samples before pulverizations [e.g., Fig. 1(b)]. The pulverization indeed introduced certain degradations to the powder-diffraction quality, which in turn prohibits us from performing unambiguous Rietveld refinements. We thus show the profile fitting result in Fig. 8(c) rather than the Rietveld refined plot as one should do for determining the actual long-range sodium ordering. Figure 9 exhibits a three-dimensional sodium-ordering model for $x=0.84$ with a simplified in-phase stacking of the Na1 monomers along c axis. Although the structural model in Fig. 9 does not signify an obvious driving force for the observed c-axis tripling [Fig. 8(c)], it does provide a tentatively plausible picture in tackling the complex ordering of the Na1 monomers in $x=0.84$. The dominance of the Na1 monomers in the long-range sodium ordering of $x=0.84$ should give structural hints to its unexpectedly comparable magnetic exchange constants in ab plane and along c axis.[12,13]

In Ref. 23, diffraction patterns similar to Fig. 1(b) have also been observed. Considering the ordering of otherwise Na1 *trimers* in the superlattice,[23] the authors proposed an associated monocliniclike superlattice (without c-axis tripling; the space group not specified), which can describe four of the 12 characteristic superlattice spots encircling the primitive $\{100\}_p$ reflections [Fig. 1(b)]. To fully account for the 12 spots, the existence of three crystallographic domains for the monocliniclike superlattice must be considered, however, not addressed in Ref. 23. In contrast, our proposed superlattice in Fig. 9 describes six of the 12 spots with a hexagonal-type repetition as shown in Fig. 1(c), and a two-domain consideration can take into account all the 12 reflections [Fig. 1(b)]. Indeed, the single-domain diffraction pattern characteristic to our superlattice was unambiguously identified in Fig. 1(c), and the estimated domain size of at least ~ 150 nm is in fair agreement with that of ~ 110 nm derived from the inverse linewidth of the x-ray superlattice reflections in Fig. 1(b). These single-domain superlattice characteristics conclusively rule out the proposed monocliniclike and Na1-trimer-based superlattice in Ref. 23 for explaining the diffraction patterns similar to Fig. 1(b). The interpretation of the superlattice in Ref. 23 may require certain revisions.

IV. CONCLUSION

Using the complementary techniques of x-ray and electron diffractions, we unambiguously established the existence of the exceptionally large superlattices in $x=0.71$ and 0.84 ($\sqrt{12}a_p \times \sqrt{12}a_p \times 3c_p$ and $\sqrt{13}a_p \times \sqrt{13}a_p \times 3c_p$) due to their respective long-range three-dimensional sodium orderings. In $x=0.71$, the sodium ordering is characterized by a spiral-like Na1-trimer chain that screws along c axis and is decorated with alternating truncated-triangle and honeycomb Na2 sublattices in ab plane. The possible origin for the long-range three-dimensional sodium ordering observed in $x=0.71$ were discussed in the frame of Coulomb repulsion consideration or the ionic potential of the Co triangular sublattices and found to be insufficient. In $x=0.84$, the superlattice is rather a result of the ordering of Na1 monomers, decorated only with truncated-triangle Na2 sublattices in ab plane. In $x=0.71$ and 0.84, their differences in the superlattices and the corresponding three-dimensional sodium ordering, dictated by the respective Na1 trimers and monomers, may provide structural hints to the drastically different magnetic ground states (a unique spin liquid state for $x=0.71$; A-type antiferromagnetic ordering for $x=0.84$) and to stimulate future experimental and theoretical explorations.

ACKNOWLEDGMENTS

This work was supported by the National Taiwan University Excellence Project and the National Science Council Taiwan. We thank Woei-Wu Pai of National Taiwan University for fruitful discussion.

*Corresponding author; chumingwen@ntu.edu.tw

[1] C. Fouassier, G. Materjka, J.-M. Reau, and P. Hagenmuller, J. Solid State Chem. **6**, 532 (1973).
[2] C. Delmas, J.-J. Braconnier, C. Fouassier, and P. Hagenmuller, Solid State Ionics **3-4**, 165 (1981).
[3] G. J. Shu, Andrea Prodi, S. Y. Chu, Y. S. Lee, H. S. Sheu, and F. C. Chou, Phys. Rev. B **76**, 184115 (2007).
[4] M.-L. Foo, Y. Wang, S. Watauchi, H. W. Zandbergen, T. He, R. J. Cava, and N. P. Ong, Phys. Rev. Lett. **92**, 247001 (2004).
[5] Q. Huang, M.-L. Foo, R. A. Pascal, Jr., J. W. Lynn, B. H. Toby, T. He, H. W. Zandbergen, and R. J. Cava, Phys. Rev. B **70**, 184110 (2004).
[6] Q. Huang, B. Khaykovich, F. C. Chou, J. H. Cho, J. W. Lynn, and Y. S. Lee, Phys. Rev. B **70**, 134115 (2004).
[7] L. Viciu, Q. Huang, and R. J. Cava, Phys. Rev. B **73**, 212107 (2006).
[8] A. J. Williams, J. P. Attfield, M. L. Foo, L. Viciu, and R. J. Cava, Phys. Rev. B **73**, 134401 (2006).
[9] H. W. Zandbergen, M. L. Foo, Q. Xu, V. Kumar, and R. J. Cava, Phys. Rev. B **70**, 024101 (2004).
[10] K. Takada, H. Sakurai, E. Takayama-Muromachi, F. Izumi, R. A. Dilanian, and T. Sasaki, Nature (London) **422**, 53 (2003).
[11] A. T. Boothroyd, R. Coldea, D. A. Tennant, D. Prabhakaran, L. M. Helme, and C. D. Frost, Phys. Rev. Lett. **92**, 197201 (2004).
[12] S. P. Bayrakci, I. Mirebeau, P. Bourges, Y. Sidis, M. Enderle, J. Mesot, D. P. Chen, C. T. Lin, and B. Keimer, Phys. Rev. Lett. **94**, 157205 (2005).
[13] L. M. Helme, A. T. Boothroyd, R. Coldea, D. Prabhakaran, D. A. Tennant, A. Hiess, and J. Kulda, Phys. Rev. Lett. **94**, 157206 (2005).
[14] M. Lee, L. Viciu, L. Li, Y. Wang, M. L. Foo, S. Watauchi, R. A. Pascal Jr., R. J. Cava, and N. P. Ong, Nature Mater. **5**, 537 (2006).
[15] M. Coey, Nature (London) **430**, 155 (2004).
[16] Q. Huang, M. L. Foo, J. W. Lynn, H. W. Zandbergen, G. Lawes, Yayu Wang, B. H. Toby, A. P. Ramirez, N. P. Ong, and R. J. Cava, J. Phys.: Condens. Matter **16**, 5803 (2004).
[17] G. Gašparović, R. A. Ott, J.-H. Cho, F. C. Chou, Y. Chu, J. W. Lynn, and Y. S. Lee, Phys. Rev. Lett. **96**, 046403 (2006).
[18] I. R. Mukhamedshin, H. Alloul, G. Collin, and N. Blanchard, Phys. Rev. Lett. **93**, 167601 (2004).
[19] I. R. Mukhamedshin, H. Alloul, G. Collin, and N. Blanchard, Phys. Rev. Lett. **94**, 247602 (2005).
[20] D. J. Singh and Deepa Kasinathan, Phys. Rev. Lett. **97**, 016404 (2006).
[21] C. A. Marianetti and G. Kotliar, Phys. Rev. Lett. **98**, 176405 (2007).
[22] F. C. Chou, M.-W. Chu, G. J. Shu, F.-T. Huang, W. W. Pai, H. S. Sheu, and P. A. Lee, Phys. Rev. Lett. **101**, 127404 (2008); W. W. Pai, S. H. Huang, Y. S. Meng, Y. C. Chao, C. H. Lin, H. L. Liu, and F. C. Chou, *ibid.* **100**, 206404 (2008).
[23] M. Roger, D. J. P. Morris, D. A. Tennant, M. J. Gutmann, J. P. Goff, J.-U. Hoffmann, R. Feyerherm, E. Dudzik, D. Prabhakaran, A. T. Boothroyd, N. Shannon, B. Lake, and P. P. Deen, Nature (London) **445**, 631 (2007).
[24] J. P. Wright, J. P. Attfield, and P. G. Radaelli, Phys. Rev. Lett. **87**, 266401 (2001).
[25] E. Wawrzyńska, R. Coldea, E. M. Wheeler, I. I. Mazin, M. D. Johannes, T. Sörgel, M. Jansen, R. M. Ibberson, and P. G. Radaelli, Phys. Rev. Lett. **99**, 157204 (2007).
[26] *International Table for Crystallography*, 5th ed., edited by Th. Hahn (Springer, Berlin, 2005), Vol. A.
[27] R. J. Balsys and R. L. Davis, Solid State Ionics **93**, 279 (1996).
[28] R. D. Shannon, Acta Crystallogr., Sect. A: Cryst. Phys., Diffr., Theor. Gen. Crystallogr. **32**, 751 (1976).
[29] F.-T. Huang, M.-W. Chu, G. J. Shu, and F. C. Chou (private communication). To the first approximation, there can be 18 stacking combinations for the $\mathbf{Q}_{1,2,3}$ and $\mathbf{T}_{1,2,3}$ sodium layers. The 18 combinations are then reduced to 13 choices by the translation operation since 5 of the 18 choices can find their crystallographic equivalent counterparts among the rest 13.
[30] J. D. Watson and F. H. C. Crick, Nature (London) **171**, 737 (1953).